A Novel Approach for Facial Symmetry Analysis Based on Semantic Registration

Narumi Kihara [1], Namiko Kimura-Nomoto [2], Takako Okawachi [3], Guangxu Li [4,5], Norifumi Nakamura [2,6], and Tohru Kamiya [1,*]

[1] Kyushu Institute of Technology, Department of Mechanical and Control Engineering, Fukuoka, Japan
[2] Department of Oral and Maxillofacial Surgery, Kagoshima University, Kagoshima, Japan
[3] National Hospital Organization Kagoshima Medical Center, Kagoshima, Japan
[4] School of Electronics and Information Engineering, Tiangong University, Tianjin, China
[5] Tianjin Medical University Eye Hospital, Tianjin, China
[6] Department of Oral and Maxillofacial Surgery, Universitas Indonesia, Jawa Barat, Indonesia
Email: kihara.narumi101@mail.kyutech.jp (N.K.); nkimura@dent.kagishima-u.ac.jp (N.K.N.); okawachi.takako.em@mail.hosp.go.jp (T.O); liguangxu@tiangong.edu.cn (G.L.); gigi1394nakamura@gmail.com (N.N.); kamiya@cntl.kyutech.ac.jp (T.K.)
*Corresponding author

***Abstract*—A cleft lip is a common congenital malformation that often has a negative impact on patients. Surgery can improve patients' quality of life, but the criteria for facial symmetry are unclear, so quantitative facial symmetry analysis is expected to make the surgery more effective. In this study, we propose a new evaluation method based on segmentation and registration using 4D data. In the segmentation step, a deep learning model divides the 3D faces into different regions, such as the upper lip and nose. In the registration process, the Coherent Point Drift (CPD) algorithm is applied to the regions of interest extracted based on the segmentation results, which simplifies the registration process. Using the registration results, the corresponding points are searched for between intra- and inter-faces. Finally, symmetry analysis is performed. Our method quantifies facial asymmetry from two perspectives: shape and movement differences. Both difference indicators are easily calculated using the point correspondences. The experimental results showed that our proposed method provided a reasonable analysis. We also discussed the relationship between segmentation accuracy and analysis quality. The results demonstrated the need to improve the segmentation to obtain better analysis results.**

***Keywords*—cleft lip, facial symmetry analysis, 3D point cloud, 4D data, segmentation, registration, deep learning, coherent point drift**

I. Introduction

Facial symmetry has been associated with psychological and physiological well-being, which are important components of Quality of Life (QoL) [1]. Congenital craniofacial disorders can affect facial symmetry [2, 3], and cleft lips are a common congenital malformation with a high prevalence reported in many population-based registries [4]. Studies have shown that the deformity of cleft lips often has a negative impact on patients [5, 6]. Therefore, surgery plays an important role in improving their QoL. In clinical practice, a system for analyzing facial symmetry is expected to make the surgeries more effective and quantitative because the criteria for facial symmetry are unclear.

Since the human face has a complex 3D structure, many previous studies have used 3D data to analyze facial symmetry. This approach has significantly evolved owing to recent advances in 3D sensor technologies, image processing techniques, and machine learning methods. By contrast, our focus is on 4D data, which contains both 3D spatial information and temporal changes. 4D data enables a more detailed analysis using not only 3D structure but also the dynamics of the face.

In this paper, we propose a novel approach for analyzing facial asymmetry using 4D data (multiple 3D point clouds containing temporal changes). The main contributions of our proposed method are as follows:

(1) We present a new framework for facial asymmetry analysis using 4D data based on semantic registration.
(2) Our method is fully automated and does not require any human interaction, making it independent of clinicians' subjective experience.

II. Literature Review

Table I shows recent studies on facial symmetry analysis for patients with cleft lips. We focus on four key components to discuss each method.

(1) Data: 3D data contains x, y, and z coordinates, whereas 4D data also contains time-series information.
(2) Method: The landmark-based method typically calculates distances between corresponding landmarks. The method is relatively easy to implement, but it lacks detail. In contrast, mesh- and

Manuscript received February 5, 2026; revised April 13, 2026; accepted May 6, 2026; published September 10, 2026.

doi: 10.18178/joig.14.5.756-762

point cloud-based methods can analyze entire specific parts or faces.

(3) Automation: This item shows whether each method is fully automated or requires human interaction.

(4) Dynamics: This item shows whether each method utilizes time-series information for analysis.

TABLE I. COMPARISON BETWEEN RELATED STUDIES AND OURS

Study	Data	Method	Automation	Dynamics
Schmutz *et al.* [7]	3D	Landmark	×	×
Martinková *et al.* [8]	3D	Landmark, Mesh	×	×
Al-Rudainy *et al.* [9]	3D	Mesh	○	×
Gattani *et al.* [10]	4D	Mesh	×	○
Kihara *et al.* [11]	4D	Landmark	○	○
Ours	4D	Point cloud	○	○

Table I lists two studies [7, 8] that used 3D data. While these studies provide valuable insights into 3D faces with cleft lips, they require the involvement of specialists to digitize the 3D landmark positions, and they are limited using 3D data. Al-Rudainy *et al*. [9] evaluated facial symmetry using 3D images of faces before and after surgical correction. Although 3D faces that were taken at different times were used, the symmetry analysis was performed on each face, and the study did not aim to evaluate facial dynamics. Gattani *et al*. [10] used 4D data and presented a detailed analysis considering the facial dynamics. However, their method requires manual digitization of facial landmarks, and the video length is limited to approximately 3 s due to the accuracy of the automatic landmark tracking. In our previous research [11], we proposed a landmark tracking method based on 3D feature descriptors and analyzed facial symmetry using its results. However, landmark-based analysis cannot provide a detailed analysis and is susceptible to accumulated errors in landmark tracking.

III. MATERIALS AND METHODS

Based on the discussion in the literature review section, we propose a fully automated, landmark-free method of analyzing facial asymmetry using 4D data. The overview is shown in Fig. 1. Our method consists of the following three steps:

(1) Facial part segmentation for each 3D point cloud based on deep learning;

(2) Non-rigid registration and pair search between intra- and inter-faces using the segmentation results;

(3) Asymmetry analysis based on two perspectives: shape and movement differences.

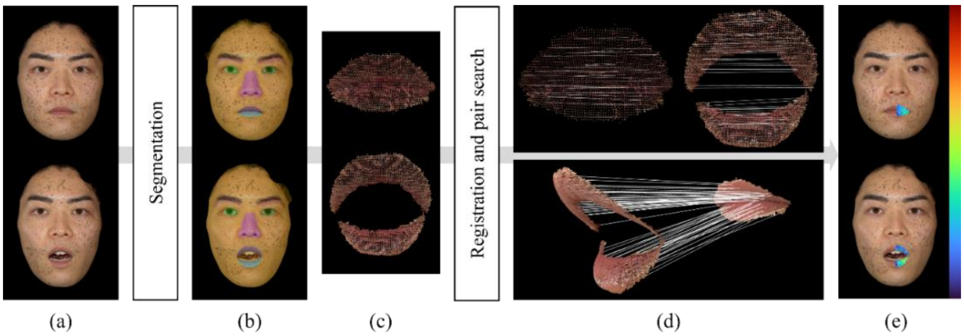

Fig. 1. Overview of our proposed method: (a) Multiple 3D point clouds as 4D data. (b) Segmentation results. (c) Regions of interest extracted using the segmentation. (d) Point matching: The upper figure shows intra-pairs and the lower one shows inter-pairs. (e) Symmetry analysis: The upper figure shows the shape difference, and the lower one shows the movement analysis.

A. Segmentation

For facial part segmentation, we build on our previous research, which presented a novel deep learning-based framework for segmentation from 3D point clouds of the face [12]. We use Point Transformer v3 (PTv3) as our segmentation model [13]. This model overcomes the trade-off between computational cost and performance, achieving high segmentation accuracy with low memory consumption.

1) Pre-training

We created a large-scale dataset of 3D faces by combining the CelebA-HQ dataset [14, 15] with 3D Dense Face Alignment V3 (3DDFA-V3) [16]. CelebA-HQ contains 2D face images, while 3DDFA-V3 reconstructs 3D faces with detailed pseudo-labels from 2D images. PTv3 is trained on this synthetic dataset, which includes 22,000 faces.

2) Fine-tuning

The pre-trained PTv3 model is further optimized using our small-scale private dataset. Details are shown in Section IV. As in the pre-training stage, pseudo-labels of facial parts are generated using 3DDFA-V3. However, we replace the upper and lower lip labels with manually created ground truth for more accurate segmentation.

B. Registration and Pair Search

1) Symmetric plane detection

Detecting a symmetric plane is an important step in comparing the left and right sides of the face. We introduce a fully automated method proposed by Hosoki *et al*. [17], which is robust to the deformity caused by cleft lips because of the removal of the perinasal and perioral regions. Specifically, by excluding these regions where severe deformities typically appear before applying the

Iterative Closest Point (ICP) [18] algorithm, it prevents the registration from converging to a local optimum. For detailed experimental validation regarding the robustness and fault-tolerance of this approach, please refer to Hosoki *et al*. [17]. Once the plane is detected, the point cloud is shifted and rotated so that it lies on the *yz* plane, positioning the face in a frontal view (Fig. 2).

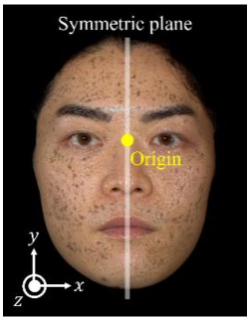

Fig. 2. Frontal face based on symmetric plane and axis directions.

2) Registration

We use the Coherent Point Drift (CPD) [19, 20] algorithm for registration. It can perform both rigid and non-rigid registration and has been widely used in many studies. The classical CPD algorithm is employed for two main reasons. First, the results of facial part segmentation are utilized to simplify the registration process, which is referred to as "semantic registration". A specific part (e.g., the upper or lower lip) is extracted as a region of interest, and non-rigid CPD is applied to this part. Second, the classical methods do not require any training, which reduces the cost for clinical applications.

3) Corresponding pair search

Point pairs are searched for between the intra- and inter-faces using the registration results. As the method of pair search is almost the same in both intra- and inter-situations, we first describe the common theoretical background.

Let C_s be a source point cloud, C_t be a target point cloud, and T be a transformation matrix estimated by non-rigid CPD. The pair search is performed between the two-point clouds C_t and C_sT. For simplicity, the transformed source cloud C_tT is denoted as C_s^T. Given a point p_s^T in the point cloud C_s^T, the pair search problem is to find its corresponding point in the target cloud. In this paper, we propose Cosine Similarity Matching (CSM) as a solution to this problem. The pseudocode of the CSM algorithm is shown in Algorithm 1.

Algorithm 1: Python-like Pseudocode of CSM

Input: C_s, C_s^T, C_t
Output: list of detected pairs P

```
for i in range (number of points in C_s):
    get p_s, p_s^T as i_th point in C_s, C_s^T, respectively
    calculate v_s by Eq. (1)
    compute KNN in C_t, given p_s^T as query
    for p_t in KNN_list:
        calculate v_t and similarity by Eqs. (2) and (3)
        if similarity is max:
            update current maximum cosine similarity
    add a pair p_s and p_t with maximum similarity to P
```

Let p_s be the original point of p_s^T (i.e., $p_s^T = p_sT$, C_s^{mask}, C_t^{mask}), CSM first calculates a shift vector v_s from p_s to p_s^T using the Eq. (1). This vector indicates the movement of the source point described by the transformation matrix.

$$v_s = p_s^T - p_s \tag{1}$$

Next, given p_s^T as a query, CSM performs the K-Nearest Neighbor (KNN) search to find neighbor points in the target cloud. Let p_t be one of the neighbor points, CSM calculates a shift vector v_s from p_s to p_t. This vector indicates the movement of a candidate pair between the source and target.

$$v_t = p_t - p_s \tag{2}$$

Then, CSM calculates the cosine similarity between two shift vectors v_s and v_t.

$$Cosine\ Similarity = \frac{v_s \cdot v_t}{\|v_s\|\|v_t\|} \tag{3}$$

These vectors v_s and v_t have the same initial point p_s and different terminal points p_s^T and p_t, respectively. If p_t is a good corresponding point for p_s^T, the cosine similarity will be close to one. Based on this idea, CSM calculates v_t and cosine similarities for all neighbor points and finds the best point that gives the largest cosine similarity. By repeating this process for all points in the source cloud, dense point pairs are obtained between the source and target.

The rest of this subsection provides details on intra- and inter-cases. The pseudocodes for each case are shown in Algorithms 2 and 3.

Algorithm 2: Python-like Pseudocode of Intra-Pair Search

Input: point cloud C, segmentation result S, id numbers of facial parts used for analysis N_{id}
Output: list of intra-pairs P

```
for i in N_id:
    get C_mask collecting points of C labeled as i in S
    extract left and right clouds from C_mask
    mirror the right cloud
    compute non-rigid CPD
    compute CSM
    add CSM result to P
```

Algorithm 3: Python-like Pseudocode of Inter-Pair Search

Input: C_s, source's segmentation result S_s, C_t, target's segmentation result S_t, N_{id}
Output: list of inter-pairs P

```
for i in N_id:
    get C_s^mask collecting points of C_s labeled as i in S_s
    get C_t^mask collecting points of C_t labeled as i in S_t
    global-registration based on centroid coordinates
    local-registration using non-rigid CPD
    compute CSM
    add CSM result to P
```

In the intra-face case, a single point cloud is used. Since the coordinates of the point clouds are standardized based on the symmetric plane, the left and right sides of the face can be easily obtained; the left cloud consists of points with negative x-coordinates, and the right cloud consists of points with positive x-coordinates. Before registration, the right cloud is mirrored by multiplying all points' x-coordinates by -1. Then, we set the mirrored right cloud as the source, and the left cloud as the target.

In the interface case, two-point clouds of the same person are used to enable analysis of facial dynamics. We set the face with an open mouth as the source, and the face with a relaxed expression as the target. In this case, the source cloud is transformed so that the source and target centroids have the same coordinates. This global registration makes the CPD algorithm more robust to facial expressions.

C. *Quantification of Shape*

The pairs between the left and right sides of the face are obtained in the inter-case. Let p_{mright} be a point in the mirrored right cloud (i.e., source), and p_{left} be its corresponding point in the left cloud (i.e., target). The shape difference D_s is calculated using the Eq. (4).

$$D_s = \left\| p_{left} - p_{mright} \right\| \tag{4}$$

D. *Quantification of Facial Expression*

This process uses both intra- and inter-faces pairs. Given an intra-pair p_t^{left} and p_t^{right} in the target cloud, their corresponding pointsp_t^{left} and p_t^{right} in the source cloud can be obtained using the inter-pairs. Then, shift vectors v_{left} and v_{right} are calculated using the following Eqs. (5) and (6).

$$v_{left} = p_t^{left} - p_s^{left} \tag{5}$$

$$v_{right} = p_t^{right} - p_s^{right} \tag{6}$$

These shift vectors indicate the movements in each facial point. To quantify the left-right difference between v_{left} and v_{right}, the vector v_{right} is mirrored by multiplying the x-coordinate of v_{right} by -1, yielding the mirrored shift vector v_{mright}. Finally, the movement difference D_m is calculated using the Eq. (7).

$$D_m = \left\| v_{left} - v_{mright} \right\| \tag{7}$$

E. *Implementation Details*

For segmentation, we followed the hyperparameters from our previous research [12]. For the CPD algorithm, we used a class named "DeformableRegistration" provided in its Python implementation [20]. We set *tolerance* = 0, max_iteration = 100, and used the other parameters at their default values. In addition, we used upper and lower lips as regions of interest for the analysis, because cleft lips are accompanied by deformities in these regions. For our CSM algorithm, the value of k for the KNN search was calculated as $k = 0.02N$, where N denotes the number of points in the given point cloud.

IV. Result and Discussion

A. *Evaluation Protocol*

Quantitatively assessing the results of facial symmetry analysis is difficult. Instead, we examine the relationship between segmentation accuracy and analysis quality. To provide a comprehensive assessment, the analysis quality is evaluated in two different ways: using Mean Absolute Error (MAE) and Unbalanced Optimal Transport (UOT) [24, 25]. The first workflow using MAE is as follows:

(1) Perform the asymmetry analysis using the segmentation result and save the D_s and D_m values of each point. (a case using the segmentation result (CASE-SEG))
(2) Perform the analysis again using the ground truth and save the results. (a case using the ground truth (CASE-GT))
(3) Extract the intersection cloud C_{int} of the segmentation result and ground truth.
(4) Given a difference indicator D (either D_s or D_m), calculate the MAE between D values of CASE-SEG and CASE-GT to evaluate the quality of the analysis. This is formulated in Eq. (8), where N_{int} denotes the number of points in C_{int}.

$$MAE = \frac{1}{N_{int}} \sum_{C_{int}} \left| D_{CASE-SEG} - D_{CASE-GT} \right| \tag{8}$$

(5) Calculate the Pearson correlation between the segmentation accuracy, Intersection over Union (IoU), and the MAE of the analysis result.

The second workflow using UOT is as follows:

(1) Retrieve the analysis results, CASE-SEG and CASE-GT, obtained in the previous steps. Unlike the MAE workflow, this method utilizes the entire point cloud without extracting the intersection cloud.
(2) Given a difference indicator D (either D_s or D_m), apply UOT to calculate the transport cost between the overall distributions of D values in CASE-SEG and CASE-GT. This transport cost serves as a global evaluation of the analysis quality.
(3) Calculate the Pearson correlation between the IoU and UOT values.

IoU is one of the most frequently used metrics for evaluating the accuracy of segmentation. Let C_{gt} be the point cloud of the ground truth, and C_{pred} be the point cloud of a deep learning model's prediction. The IoU is calculated using their intersection and union sets, as shown in Eq. (9). The value of IoU ranges from 0 to 1, and the larger it is, the more accurate the prediction.

$$IoU = \frac{C_{gt} \cap C_{pred}}{C_{gt} \cup C_{pred}} \tag{9}$$

B. Dataset

The details of our private dataset are shown in Table II. These point clouds were captured at Kagoshima University in Japan using a VECTRA H1 Camera (Canfield Scientific). For Table II group (a), the participants were asked to sit on a chair with a relaxed expression. For Table II groups (b) and (c), the participants were also asked to open their mouths, and an additional 1 to 3 point clouds were captured. In total, our dataset consists of 55-point clouds including multiple facial expressions of the same subjects.

TABLE II. DETAILS OF THE PRIVATE DATASET

Group	Cleft Lip	Subjects	Total Data
(a)	with	15	15
(b)	with	8	21
(c)	without	5	19

C. Result and Discussion

The asymmetry analysis was performed for 13 subjects whose facial dynamics were available. Examples of the analysis are shown in Fig. 3. For these visualizations, the colors were obtained using the Turbo colormap [22] according to the values of the difference indicators at each point.

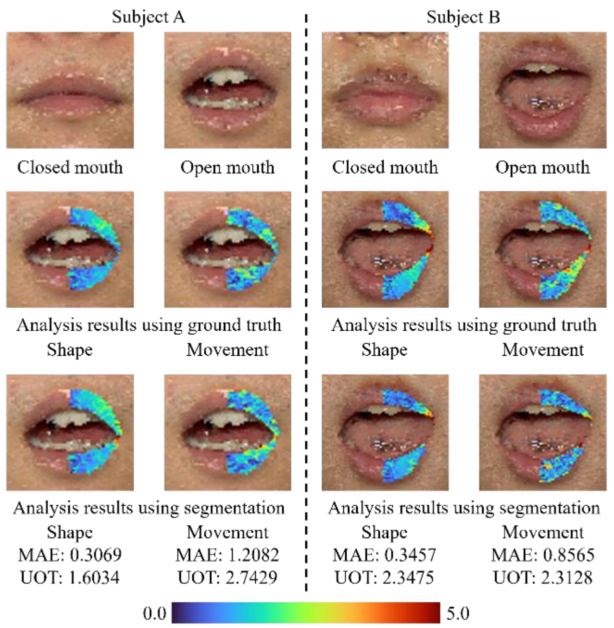

Fig. 3. Analysis results of two different subjects. We refer to the subject on the left side as A, the subject on the right side as B. The colormap shows the corresponding values of indicators. Note that for enhanced visibility, the discrete 3D point clouds have been rendered as continuous 2D images.

The analysis result using the ground truth of subject A shows that there is no significant asymmetry in either shape or movement differences. Compared with this, the analysis result using segmentation (IoU: upper lip = 0.844, lower lip = 0.780) produces a large MAE and UOT especially in the D_m values. This is possibly because two-point clouds are used to calculate D_m, making it more sensitive to the segmentation accuracy.

The figure of subject B in Fig. 3 shows an example of an extreme facial expression. We can see that there is a large left-right difference in the corner of the mouth, which is also evident in the analysis result using the ground truth. However, the segmentation-based analysis does not produce good results due to the low prediction accuracy (IoU: upper lip = 0.656, lower lip = 0.839). Avoiding erroneous connectivity between the upper and lower lips in the segmentation of 3D faces is challenging but crucial to providing a reliable analysis. Furthermore, when such topological segmentation failures occur, calculating errors based solely on the intersection area become less reliable, highlighting the need for a more robust evaluation metric based on overall distributions.

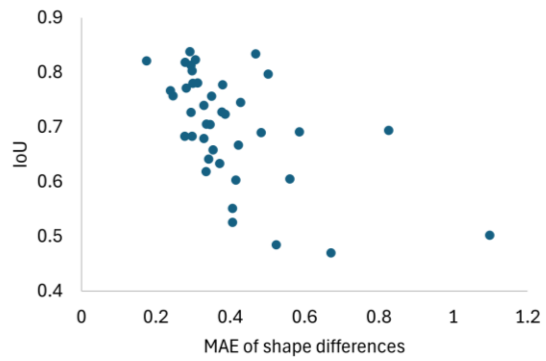

Fig. 4. Scatter plot on shape differences.

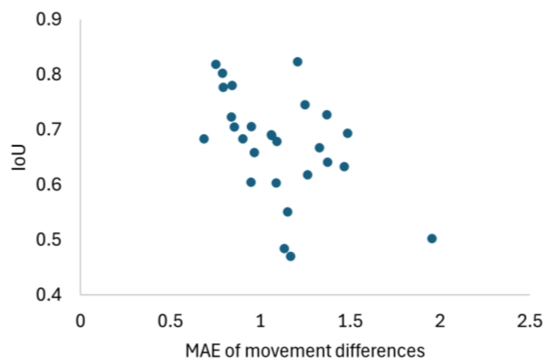

Fig. 5. Scatter plot on movement differences.

Figs. 4 and 5 show the scatter plots of IoU and MAE. The Pearson correlations between these metrics are −0.5535 for Fig. 4 and −0.4714 for Fig. 5. In general, these values suggest a weak negative correlation [21] between IoU and MAE; the lower the IoU, the larger the MAE. To overcome the limitations of MAE, we introduced UOT as an additional metric. Figs. 6 and 7 show the scatter plots of IoU and UOT. By employing UOT distance based on overall distributions, the Pearson correlations showed a stronger negative correlation: −0.7454 for shape differences and −0.7489 for movement differences. This dramatic improvement shows that UOT effectively identifies the severe structural errors caused by poor segmentation, which MAE overlooked.

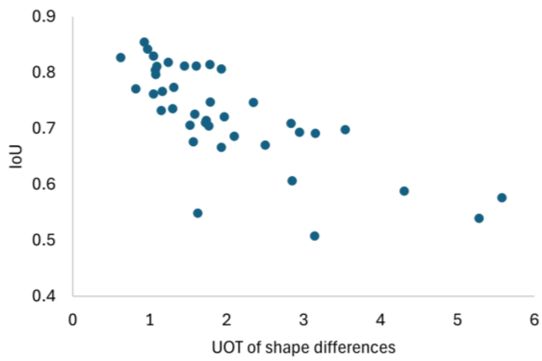

Fig. 6. Scatter plot on shape differences.

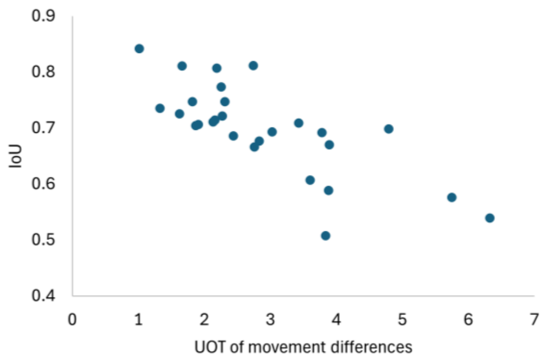

Fig. 7. Scatter plot on movement differences.

Based on the above qualitative and quantitative discussions, we conclude that our proposed method shows great potential as a new approach to facial symmetry analysis, while the improvement in segmentation accuracy is essential for clinical use. To address this issue, it is crucial to enhance the extraction of geometric features, such as the boundaries of the lips. For instance, the contour wavelet-based approach proposed by Zhang *et al*. [23] provides valuable insights into our future work to design more effective loss functions and improve the segmentation network.

V. Conclusion

In this paper, we propose a novel method for analyzing facial symmetry that uses deep learning-based segmentation and CPD-based registration. Our method was designed to work automatically and utilize facial dynamics. The experimental results showed that the asymmetric areas were evaluated with large left-right differences.

We discuss the limitations and future work as follows:

Improvement in face segmentation: The results showed the negative Pearson correlation between segmentation accuracy and analysis quality error, suggesting the need to improve the segmentation accuracy. As discussed in the previous section, enhancing the extraction of geometric features will be a critical step to achieving this goal.

Wider region of interest: For this study, we selected only the upper and lower lips as regions of interest. However, cleft lips are often accompanied by deformities in the nasal and philtra areas. While our method cannot currently analyze these areas, we believe it can easily be expanded to include regions beyond the lips. Specifically, by using the segmentation results of the nose, upper lip, and lower lip, we can define a 3D bounding box to construct a broader spatial region of interest. Extracting all points within this cuboid will inherently include the nasal and philtra areas, allowing our proposed registration and matching framework to be directly applied for evaluating these extended facial regions.

Clinical application: Our private dataset currently consists of 55-point clouds including data from 28 subjects. Facial dynamics are available for 13 of these subjects. In the future, we plan to collect additional data to improve segmentation accuracy and provide clinically meaningful insights. Specifically, we intend to deepen our collaboration with clinical partners to encompass a broader range of cases, spanning various age groups and degrees of cleft lip severity. This continuous dataset expansion will be crucial to further validate the reliability, robustness, and generalization capabilities of our proposed method. Furthermore, the visualization colormaps generated by our system provide an objective baseline that highlights subtle structural and dynamic asymmetries. By leveraging our deepened collaboration with clinical professionals, we will explore how to translate these quantitative difference indicators into concrete reference metrics, such as specific surgical incision designs or required tissue repositioning volumes, to directly guide plastic surgeons in developing more effective surgical plans.

Quantitative discussion and performance comparison: In this study, we evaluated the relationship between segmentation accuracy and analysis quality using both MAE and UOT. By introducing UOT based on overall distributions, we effectively addressed the limitation of MAE, which relies solely on the intersection area. However, our current quantitative evaluation is limited to validating the proposed framework itself. Therefore, it is essential to conduct a quantitative performance comparison against other existing methods, such as landmark- or mesh-based systems commonly used in clinical practice. To more clearly demonstrate the advantages of our proposed method, it will be necessary to compare dimensions such as computation time, analysis error, and operational complexity.

Conflict of Interest

The authors declare no conflict of interest.

Author Contributions

Narumi Kihara conducted the research and wrote the paper. Namiko Kimura-Nomoto and Takako Okawachi collected the facial data, verified the quality of the ground truth, and examined the research from a medical perspective. Guangxu Li, Norifumi Nakamura, and Tohru Kamiya acted as academic supervisors and reviewed the research in terms of engineering, computer vision, and medical imaging. All authors have approved the final version.

FUNDING

This work was supported by JST SPRING, Japan Grant Number JPMJSP2154.

REFERENCES

[1] T. K. Shackelford and R. J. Larsen, "Facial asymmetry as an indicator of psychological, emotional, and physiological distress," *J. Pers. Soc. Psychol.*, vol. 72, no. 2, pp. 456–466, 1997.

[2] A. M. Paradowska-Stolarz, M. Ziomek, and K. Sluzalec-Wieckiewicz, "Most common congenital syndromes with facial asymmetry: A narrative review," *Dent. Med. Probl.*, vol. 61, no. 6, pp. 925–932, 2024.

[3] T. M. Choi *et al*., "Automated three-dimensional analysis of facial asymmetry in patients with syndromic coronal synostosis: A retrospective study," *J. Cranio-Maxillofac. Surg.*, vol. 52, no. 1, pp. 48–54, 2024.

[4] International Clearinghouse for Birth Defects Surveillance and Research. (2014). Annual report 2014. [Online]. Available: http://www.icbdsr.org/wp-content/annual_report/Report2014.pdf

[5] O. Hunt, D. Burden, P. Hepper, M. Stevenson, and C. Johnston, "Self-reports of psychosocial functioning among children and young adults with cleft lip and palate," *Cleft Palate-Craniofac. J.*, vol. 43, no. 5, pp. 598–605, 2006.

[6] A. Paganini, M. Persson, and H. Mark, "Influence of gender, dispositional optimism, and coping strategies on appearance-related distress among Swedish adults with cleft lip and palate," *Cleft Palate-Craniofac. J.*, vol. 59, no. 6, pp. 715–723, 2021.

[7] S. Schmutz, N. Gkantidis, A. Brudnicki, and P. S. Fudalej, "Nasolabial shape and aesthetics in patients with cleft lip and palate: Analysis of 3D facial images," *Eur. J. Orthodont.*, vol. 47, no. 4, cjaf051, 2025.

[8] K. Martinková *et al*., "From infancy to toddlerhood: A 3D analysis of facial asymmetry in children with and without orofacial clefts," *Clin. Oral Invest.*, vol. 29, no. 8, 394, 2025.

[9] D. Al-Rudainy, X. Ju, S. Stanton, F. V. Mehendale, and A. Ayoub, "Assessment of regional asymmetry of the face before and after surgical correction of unilateral cleft lip," *J. Cranio-Maxillofac. Surg.*, vol. 46, no. 6, pp. 974–978, 2018.

[10] S. Gattani, X. Ju, T. Gillgrass, A. Bell, and A. Ayoub, "An innovative assessment of the dynamics of facial movements in surgically managed unilateral cleft lip and palate using 4D imaging," *Cleft Palate-Craniofac. J.*, vol. 57, no. 9, pp. 1125–1133, 2020.

[11] N. Kihara, N. Kimura-Nomoto, T. Okawachi, G. Li, N. Nakamura, and T. Kamiya, "Facial symmetry analysis for cleft lip patients from 4D point cloud data," in *Proc. Int. Conf. Control, Autom. Syst.*, 2023, pp. 1502–1505.

[12] N. Kihara, N. Kimura-Nomoto, T. Okawachi, G. Li, N. Nakamura, and T. Kamiya, "A novel deep learning-based approach for facial part segmentation from 3D point cloud data," in *Proc. Int. Conf. Comput. Pattern Recognit.*, 2025, pp. 137–145.

[13] X. Wu *et al*., "Point Transformer V3: Simpler, faster, stronger," in *Proc. IEEE/CVF Conf. Comput. Vis. Pattern Recognit.*, 2024, pp. 4840–4851.

[14] Z. Liu, P. Luo, X. Wang, and X. Tang, "Deep learning face attributes in the wild," in *Proc. IEEE Conf. Comput. Vis.*, 2015, pp. 3730–3738.

[15] T. Karras, T. Aila, S. Laine, and J. Lehtinen, "Progressive growing of GANs for improved quality, stability, and variation," arXiv Preprint, arXiv:1710.10196, 2017.

[16] Z. Wang, X. Zhu, T. Zhang, B. Wang, and Z. Lei, "3D face reconstruction with the geometric guidance of facial part segmentation," in *Proc. IEEE/CVF Conf. Comput. Vis. Pattern Recognit.*, 2024, pp. 1672–1682.

[17] D. Hosoki, T. Kamiya, N. Kimura-Nomoto, T. Okawachi, E. Nozoe, and N. Nakamura, "Symmetric plane detection and symmetry analysis from a 3D point cloud data of face," in *Proc. Int. Conf. Control, Autom. Syst.*, 2020, pp. 402–406.

[18] P. J. Besl and N. D. McKay, "A method for registration of 3-D shapes," *IEEE Trans. Pattern Anal. Mach. Intell.*, vol. 14, no. 2, pp. 239–256, 1992.

[19] A. Myronenko and X. Song, "Point set registration: Coherent point drift," *IEEE Trans. Pattern Anal. Mach. Intell.*, vol. 32, no. 12, pp. 2262–2275, 2010.

[20] A. A. Gatti and S. Khallaghi, "PyCPD: Pure NumPy implementation of the coherent point drift algorithm," *J. Open Source Softw.*, vol. 7, no. 80, 4681, 2022.

[21] P. Schober, C. Boer, and L. A. Schwarte, "Correlation coefficients: Appropriate use and interpretation," *Anesth. Analg.*, vol. 126, pp. 1763–1768, 2018.

[22] A. Mikhailov. (2019). Turbo, an improved rainbow colormap for visualization. *Google AI Blog*. [Online]. Available: https://research.google/blog/turbo-an-improved-rainbow-colormap-for-visualization/

[23] D. Zhang, J. Li, Z. Chen *et al*., "Efficient image generation with contour wavelet diffusion," *Comput. Graph.*, vol. 124, 104087, 2024.

[24] L. Chizat, G. Peyré, B. Schmitzer *et al*., "Scaling algorithms for unbalanced transport problems," *Math. Comput.*, vol. 87, pp. 2563–2609, 2018.

[25] R. Flamary, N. Courty, A. Gramfort *et al*., "POT: Python optimal transport," *J. Mach. Learn.*, vol. 22, no. 78, pp. 1–8, 2021.